Numerical Simulation of Nonlinear Structures in Channel Flow Transition

S. Biringen*
University of Colorado
Boulder, Colorado

Introduction

THE objective of this computational study is to investigate the development of nonlinear vortical structures in plane channel flow transition by the visualization of three-dimensional vortex lines. It has long been recognized that transition may be viewed as a sequence of events that is triggered by two-dimensional Tollmien-Schlichting waves that become three-dimensional, leading to nonlinear wave interactions. In a recent experiment, Williams[1] used hot film probes in a water channel boundary layer to create a data base containing three-dimensional instantaneous velocity and vorticity components documenting the evolution of the high shear layer and the formation of hairpin vortices. He then used this data base to obtain three-dimensional vortex lines. In this work, a similar technique is used to visualize the flowfield structures. In order to extract information from the computational data base, which provides the three-dimensional instantaneous velocity/vorticity field in over a quarter million grid points, vortex lines were calculated at time intervals that can be viewed sequentially. In addition, vorticity contours and velocity vector plots for the secondary flow are presented for a comparison with the findings inferred from the vortex line plots. Although flow visualization by vortex lines have been utilized in other numerical studies,[2-4] the present results effectively capture the continuous evolution of the flow, enabling the identification of various vortical structures.

Calculation Procedure

The calculation procedure for the velocity field uses the incompressible Navier-Stokes equations in primitive-variable, energy-conserving form along with the continuity equation. These equations were numerically integrated by a semi-implicit, pseudospectral method with $x_2 = \pm 1$ corresponding to the walls of the channel; second-order finite differences were employed along the wall normal direction. In this solution procedure, the flowfield is assumed to be periodic along x_1 and x_3 with the computational box length equal to 2π along these directions. Initial conditions consisted of finite-amplitude two- and three-dimensional solutions of the Orr-Sommerfeld equation corresponding to the least stable mode for $\alpha = 1$ and $\beta = 1$, where α and β are the fundamental wavelengths along x_1 and x_3, respectively. The initial maximum amplitudes normalized with channel centerline velocity were 0.10 for the 2D disturbance and 0.11 for the 3D disturbance. The computations were performed across the whole channel with no-slip boundary conditions imposed at the solid walls at $x_2 = \pm 1$. The solution procedure was vectorized and the computations were performed on the NASA/Langley VPS32 vector processor using 64-bit arithmetic on a $64 \times 63 \times 64$ mesh at a Reynolds number $Re = 1500$. Note that this Reynolds number is based on the channel half-thickness and the channel centerline velocity and is linearly stable for this flow. Details of this procedure are available elsewhere[5]; a discussion of some results from this data base is presented by Biringen.[2]

Presented as Paper 88-0404 at the AIAA 26th Aerospace Sciences Meeting, Reno, Nevada, Jan. 11-14, 1988; received Aug. 25, 1988; revision received May 4, 1989.

*Associate Professor, Department of Aerospace Engineering Sciences.

The capability and the accuracy of the numerical model were tested and demonstrated by comparisons with the linear theory for both 2D and 3D disturbances on a $16 \times 63 \times 16$ mesh. In this verification study for a range of Reynolds numbers, the amplitude errors for both 2D and 3D disturbances remained less than 1%. It can therefore be asserted that the present numerical model is free of any significant dissipative truncation errors and is indeed an accurate means of tracking the time evolution of Orr-Sommerfeld eigenvalues for plane Poiseuille flow.

An iterative procedure based on a second-order Runge-Kutta scheme was used to calculate the 3D vortex lines.

Results and Discussion

We assume the initial undisturbed flow to consist of infinitesimal spanwise vorticity sheets that can be constructed from vortex lines originating at a fixed x_2 location. In purely laminar, 2D base flow, a vortex line originating at an arbitrary location in the flowfield will always remain perpendicular to the flow direction at a constant distance from the wall. In the presence of flow excitation, the deformation of these vortex sheets demonstrates the mechanisms involved in the transition process.

Figures 1a-1g present the time evolution of a vortex sheet originating at $x_2 = -0.76$. Each of these figures was plotted over one wavelength (2π) in the spanwise direction and two wavelengths (4π) in the streamwise direction between the lower wall of the channel ($x_2 = -1$) and the channel centerline ($x_2 = 0$). This allows the vortical structures to be viewed completely when the streamwise component stretches the structure beyond a single wavelength. We note that the vortex lines

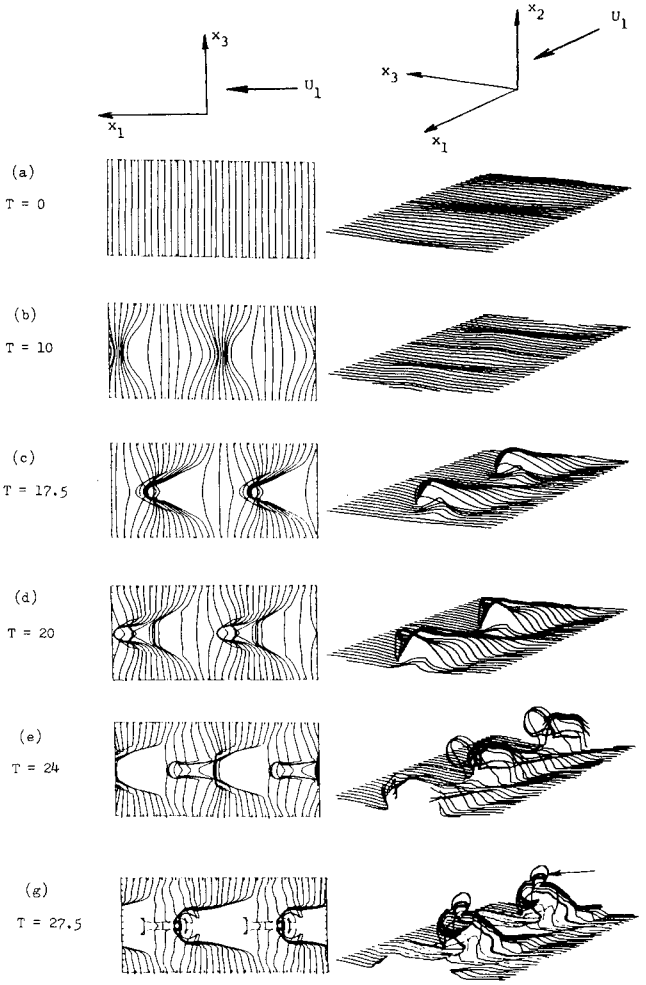

Fig. 1 Time evolution of three-dimensional vortex lines originating at $x_2 = -0.76$; $0 \le x_1 \le 4\pi$, $0 \le x_3 \le 2\pi$, $-1.0 \le x_2 \le 0$.

forming at this sheet are initially perpendicular to the flow and parallel to the wall (Fig. 1a). At $T=10.0$ (Fig. 1b), the vortex sheet has formed a well-defined vortical structure and begins to develop an out-of-plane component as the flow evolves from $T=10.0$ to $T=17.5$ (first-spike stage, Fig. 1c). This is followed by the formation of a vortex loop as the cross-channel vorticity intensifies.[5] The first spike appears to be the critical point in the development of the vortex loop as this initial uplift is almost immediately elongated in the streamwise direction. At $T=20.0$ (Fig. 1d), the first fully developed vortex loop can be depicted. It should be noted that, in these plots, the elongation of the vortex lines takes place over almost the entire sheet. As this first-born vortex loop continues to elongate in the streamwise direction, at $T=24.0$ (Fig. 1e), it forms an almost perfect horseshoe shape. This is accompanied by a secondary vortex loop appearing along the legs of the first-born vortex loop. The first-born loop continues to elongate, and at $T=27.5$ (Fig. 1g) it forms a vortex ring (indicated by the arrow) inclined at about 45 deg to the vortex axis curling into the flow. The development of vortex rings from the stretching of hairpin vortices have been first observed by Head and Bandyopadhyay[6] in turbulent boundary layers. Furthermore, in a numerical study Moin et al.[7] showed that a vortex ring can form from the induced motion of an isolated hairpin, lending support to the findings. However, the confirmation of the present results awaits a higher resolution simulation currently in progress.

The existence of the vortical structure inferred from the vortex line plots is also apparent in Fig. 2, where we plot velocity vectors of the secondary flow at $T=27.5$. The sequential examination of the u_2-u_3 velocity vectors reveals the rotational flow along the vortex axis and maps the vortex structure that loops around $x_1=3L_1/8$. In this figure, the parameter L_1 is the computational box length along x_1, i.e., $L_1=2\pi$. In Figs. 3 and 4, we present contour plots of $\partial u_1/\partial x_2$ (corresponding to approximate spanwise vorticity) and streamwise vorticity at planes passing through the peak. It is interesting to note that all the contours are smooth, and solution deterioration due to inadequate mesh resolution documented by Krist and Zang[8] is not evidenced in these figures. This may be due to the 64-bit arithmetic used in the present work as opposed to the 32-bit arithmetic used by Krist and Zang,[8] which will cause larger truncation errors. In fact, the contour plots presented here are not too different from their high-resolution simulations. We infer from the spanwise vortex contours that the shear layers forming at the lower wall (positive contours, solid lines) and those forming at the upper wall (negative contours, dashed lines) strongly interact with

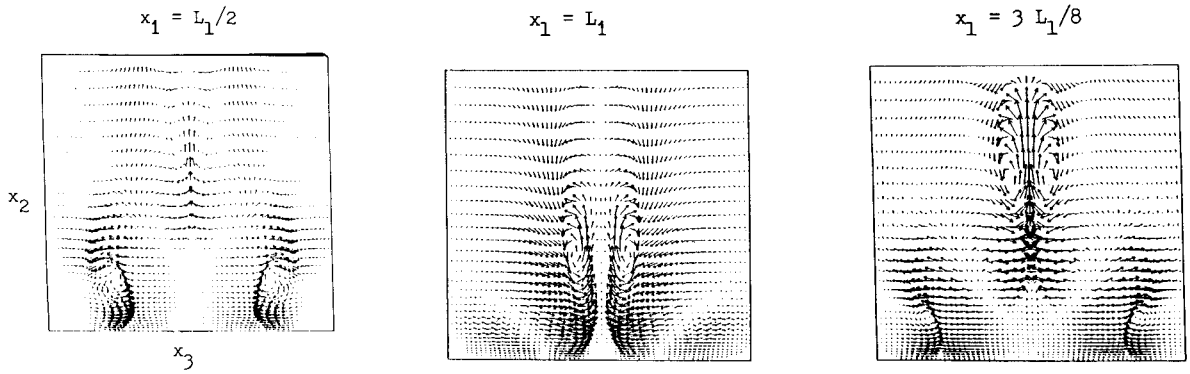

Fig. 2 Velocity vectors, u_2-u_3, indicating rotational secondary flow at $T=27.5$; $-1.0\le x_2\le 0$, $0\le x_3\le 2\pi$; flow direction is normal to the plane of the paper.

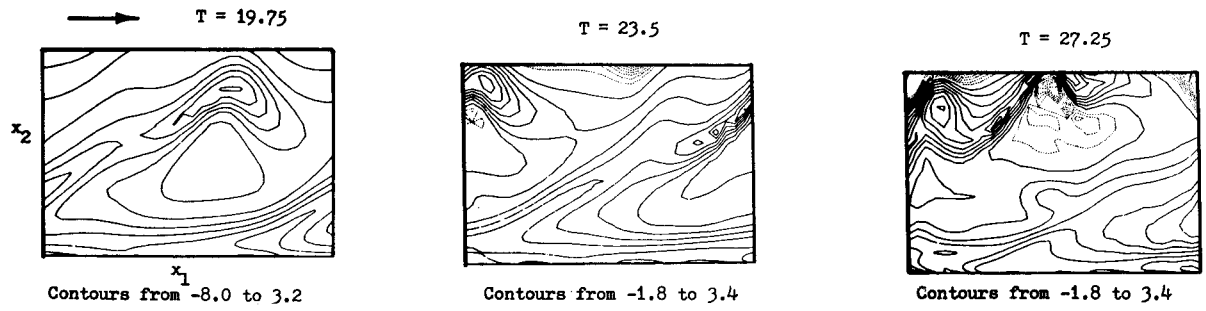

Fig. 3 Contour plots of $\partial u_1/\partial x_2$ at the peak plane; arrow indicates flow direction, and $0\le x_1\le 2\pi$, $-1.0\le x_2\le 0$. Solid lines are positive and dashed lines are negative contours.

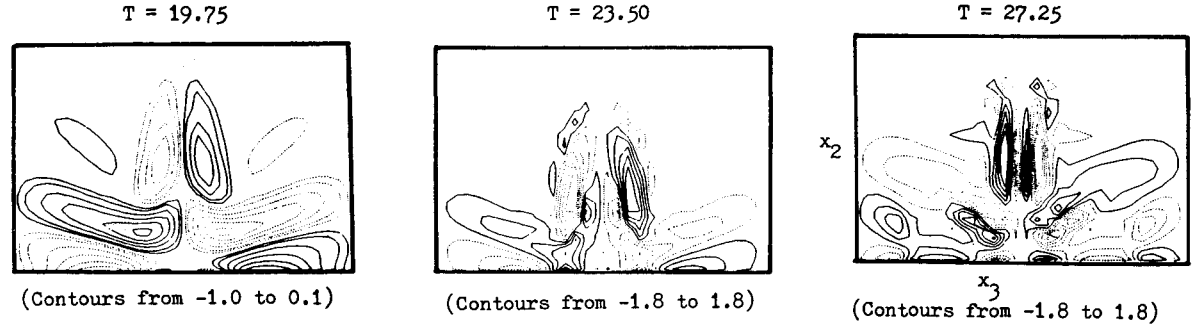

Fig. 4 Streamwise vorticity contours at the peak plane; $-1.0\le x_2\le 0$, $0\le x_3\le 2\pi$. Flow direction is normal to the plane of the paper. Solid lines are positive and dashed lines are negative contours.

each other. In their computational study, Zang et al.[3] also captured the interaction between opposing shear layers, but they infer that the incipient hairpin vortex in the lower half of the channel is "swallowed" by the counter-rotating vorticity due to the shear layer in the upper half. In the present calculations we do not observe this swallowing effect. As evident from the vortex line plots, our results point toward the full development of the lambda vortex and the hairpin vortex. Finally, Fig. 4 presents streamwise vorticity contours at fixed x_1 locations corresponding to the tip of the hairpin and displays the evolution of this vortical structure already depicted from the vortex-line plots and the velocity vectors. At later times, the streamwise vorticity contours reveal the development of several pairs of counter-rotating vortices instigated from the breakdown of the primary vortex.

Concluding Remarks

In this work, channel flow transition is visualized through the use of vortex lines representing vortex sheets. These vortex lines track the evolution of nonlinear structures, which manifest themselves as vortex tubes and hairpin vortices.

References

[1]Williams, D. R., "Vortical Structures in Breakdown Stage of Transition," *ICASE/NASA Workshop on Stability of Time-Dependent and Spatially Varying Flows,* D. L. Dwoyee and M. Y. Hussaini, eds., Springer-Verlag, New York, 1985.

[2]Biringen, S., "Three-Dimensional Structures of Transition in Plane Channel Flows," *Physics of Fluids,* Vol. 30, Nov. 1987, pp. 3359-3368.

[3]Zang, T. A., Krist, S. E., Erlebacher, G., and Hussaini, M. Y., "Nonlinear Structures in the Later Stages of Transition," AIAA Paper 87-1024, 1987.

[4]Gilbert, N. and Kleiser, L., "Near-Wall Phenomena in Transition to Turbulence," Zoran Zaric International Seminar on Near-Wall Turbulence, Dubrovnik, Yugoslavia, May 16-20, 1988.

[5]Biringen, S., "Final Stages of Transition to Turbulence in Plane Channel Flow," *Journal of Fluid Mechanics,* Vol. 148, Nov. 1984, pp. 413-442.

[6]Head, M. R. and Bandyopadhyay, P., "New Aspects of Turbulent Boundary-Layer Structure," *Journal of Fluid Mechanics,* Vol. 107, June 1981, pp. 297-338.

[7]Moin, P., Leonard, A., and Kim, J., "Evolution of a Curved Vortex Filament Into a Vortex Ring," *Physics of Fluids,* Vol. 29, April 1986, pp. 955-963.

[8]Krist, S. E. and Zang, T. A., "Numerical Simulation of Channel Flow Transition," NASA TP-2667, April 1987.

Acknowledgment

This work was performed under Grant NAG-1-798 from NASA Langley Research Center.

Control of Natural Laminar Instability Waves on an Axisymmetric Body

Daniel M. Ladd*
Naval Ocean Systems Center
San Diego, California

Introduction

THE response of a two-dimensional laminar boundary-layer instability (so called Tollmien-Schlichting, or TS, waves) to wave superposition has been the subject of several recent investigations. Liepmann et al.[1] demonstrated the generation of artificial TS waves on a flat plate using periodic pulsing of heaters embedded in a flat plate in water. Later, Liepmann and Nosenchuck[2] used this technique to actively attenuate the "naturally" occurring TS waves and to increase the length of laminar flow on the flat plate. Gedney[3] used plate vibration to attenuate sound-produced artificial TS waves. Thomas[4] used two vibrating ribbons on a flat plate in air. Milling[5] performed a similar operation with vibrating ribbons in a water channel. Except for Liepmann and Nosenchuck,[2] all of these experiments used artificially produced TS waves. The logical progression of this technique is the ability to deal with random disturbances, as would be found in most flows of interest. This experiment addresses that problem.

Received Dec. 15, 1988; presented as Paper 89-0037 at the 27th Aerospace Sciences Meeting, Reno, NV, Jan. 8-12, 1989; revision received May 26, 1989.

*Hydrodynamicist. Member AIAA.

Experimental Apparatus

The facility used was the Naval Ocean Systems Center high-speed water tunnel. This tunnel has a 305-mm circular open jet, where velocities up to 15 m/s are possible. The turbulence level (u'/U_∞) is a respectable 0.16% throughout the speed range.

The axisymmetric body used was a 9:1 fineness ratio ellipsoid of revolution. The diameter of the midsection was 50 mm. The ellipsoid maintained a true elliptical outline until an axial distance (x) of 397 mm, at which point constant slope was maintained to intercept the support diameter of 25.4 mm. The pressure distribution of this model is similar to a Reichardt body and is very flat, making this model essentially the axisymmetric equivalent of a flat plate. Previous experiments with identically shaped models have shown transition Reynolds numbers of about 2.8 million, which agrees well with the measured 0.16% turbulence level of the tunnel.

It was found that the "natural" TS waves occurring on this body would form wave packets, whose phase and amplitude were random. For the case presented here, the frequencies of the wave packets ranged from approximately 700 to 1400 Hz. The origin of these waves was presumably from the background freestream turbulence of the tunnel (hence the term "natural" as opposed to artificially produced). Comparison with spatial linear stability theory showed the center of the TS wave frequency spectrum to follow the upper branch of the linear stability curve. This is expected behavior for a body with a flat pressure distribution, whose stability curve is essentially unchanged with axial location. At frequencies higher than the center frequency, the TS waves are being damped, eventually to be of no concern. Frequencies lower than center are still in the process of being amplified, yet to reach overall peak amplification. The center frequency has reached its peak amplification and is about ready to be damped (e.g., zero amplification rate, the upper branch of the stability curve).

Method and Results

The control of randomly occurring TS waves requires a sensor before or coincident with the control actuator. Here the sensors are flush-mounted hot films. This model had the control actuator at a location well downstream from the nose. This allowed an ambient TS wave to amplify enough such that a shear-stress sensor could reasonably be expected to sense the presence of a TS wave before arriving at the actuator. This requires an actuator that can produce large control perturbations.

Our goal for an actuator design was to be able to produce a perturbation of 1% of freestream velocity at a frequency of 1000 Hz. Initial attempts at using a strip heating element as in Ref. 6 failed to produce a survivable heater element that could produce the required perturbation. A different design was tried that used a small commercially available acoustic speaker with a 21.6-mm stainless-steel diaphragm. This speaker fit conveniently inside the model, with the diaphragm perpendicular to the model axis. The function of the speaker diaphragm was to change the volume of a small cavity inside the model, to produce suction/blowing through a circumferential slot, oriented normal to the flow. The slot wide was about